Journal of
Synchrotron
Radiation

ISSN 1600-5775

Received 21 May 2014
Accepted 13 October 2014

Structure and effects of annealing in colloidal matrix-free Ge quantum dots

Yuanpeng Zhang,[a]* Ali Karatutlu,[a,b] Osman Ersoy,[a] William Little,[a] Giannantonio Cibin,[c] Andy Dent[c] and Andrei Sapelkin[a]

[a]School of Physics and Astronomy, Queen Mary, University of London, Mile End Road, London E1 4NS, UK, [b]Electrical and Electronics Engineering, Yildirim Campus, Bursa Orhangazi University, 16245 Yildirim, Bursa, Turkey, and [c]Diamond Light Source Ltd, Didcot, Oxon OX11 0DE, UK. *E-mail: yuanpeng.zhang@qmul.ac.uk

The structure of small (2–5 nm) Ge quantum dots prepared by the colloidal synthesis route is examined. Samples were synthesized using either GeO_2 or $GeCl_4$ as precursor. As-prepared samples were further annealed under Ar or H_2/Ar atmosphere at different temperatures in order to understand the effect of annealing on their structure. It was found that as-prepared samples possess distinctly different structures depending on their synthesis route as indicated by their long-range ordering. An appreciable amount of oxygen was found to be bound to Ge in samples prepared with GeO_2 as a precursor; however, not for $GeCl_4$. Based on combined transmission electron microscope, Raman, X-ray diffraction and X-ray absorption measurements, it is suggested that as-prepared samples are best described by the core-shell model with a small nano-crystalline core and an amorphous outer layer terminated either with oxygen or hydrogen depending on the synthesis route. Annealing in an H_2Ar atmosphere leads to sample crystallization and further nanoparticle growth, while at the same time reducing the Ge—O bonding. X-ray diffraction measurements for as-prepared and annealed samples indicate that diamond-type and metastable phases are present.

Keywords: Ge quantum dots (QDs); annealing; matrix-free; combined characterization; core-shell model.

1. Introduction

The synthesis, properties and applications of group IV nanoparticles have attracted great interest over the past several years (Fan & Chu, 2010). The size tunable optical and electric properties make Ge and other group IV elements including Si and C attractive for multi-junction solar cells (Cánovas *et al.*, 2010; Guter *et al.*, 2009), photodectors (Assefa *et al.*, 2010) and field-effect transistors (Pillarisetty, 2011; Kamata, 2008). Moreover, potential applications of Ge nanocrystals (NCs) on printing electronics (Kim *et al.*, 2010) and organic–inorganic hybrid photoelectric devices (Xue *et al.*, 2011) as well as in biological imaging (Lambert *et al.*, 2006, 2007) have been reported.

Ge is an indirect band semiconductor with a large exciton Bohr radius [24 nm for bulk Ge (Xue *et al.*, 2011)], leading to strong quantum confinement effects [which affects the size of the band gap and hence the light emission wavelength (Einevoll, 1992; Brus, 1983)] to be observed for relatively large particle sizes. Besides quantum confinement effects, Ge NCs can exhibit a variety of metastable structures (Ribeiro & Cohen, 2000; Yin & Cohen, 1980; Jamieson, 1963), but size-dependent structural metastability in Ge NCs has not been studied extensively as yet. This may be an interesting subject as the difference in lattice structure leads to a distinctive energy band structure, which in turn affects the light emission and absorption behaviour. For example, Ge with ST12 phase has been predicted to possess a direct band gap of 1.47 eV (Joannopoulos & Cohen, 1973) (in contrast to an indirect band gap of 0.66 eV in diamond-type Ge) with potential applications in infrared opto-electronic and photovoltaic devices (Kim *et al.*, 2010).

Until recently, most Ge quantum dots (QDs) were synthesized in a matrix (Welham, 2000; Stavarache *et al.*, 2011; Alkis *et al.*, 2012; Henderson *et al.*, 2010) or on surfaces (Cojocaru *et al.*, 2007; Desnica *et al.*, 2008; MacLeod *et al.*, 2012); however, matrix-free Ge QDs could provide a very useful model to test a variety of structural characterization methods. Hence several synthesis methods have been developed to produce matrix-free Ge QDs by etching (Muthuswamy *et al.*, 2012; Yang, 2007; Kartopu *et al.*, 2003, 2008), sol–gel synthesis (Nogami & Abe, 1997) and colloidal synthesis (Chou *et al.*, 2009; Wu *et al.*, 2011; Heath *et al.*, 1994). Colloidal synthesis methods seem to give a reasonably scalable route to volume production of Ge QDs

and provide a degree of control over particle size (Hope-Weeks, 2003; Wu *et al.*, 2006; Zaitseva *et al.*, 2007; Prabakar *et al.*, 2010) and surface termination (Fok *et al.*, 2004; Chiu *et al.*, 2005; Gerung *et al.*, 2005; Dag *et al.*, 2012). The latter is particularly crucial in matrix-free Ge QDs as surface termination significantly influences the stability of nanoparticles in various environments. In particular, hydrogen-terminated Ge may be the preferred option as it shows good aqueous stability (Peng *et al.*, 2011; Park *et al.*, 2008) and is usually a first starting point for subsequent wet and dry surface passivation (Rivillon *et al.*, 2005). Two relatively straightforward bench-top colloidal synthesis methods have been reported recently. These methods use GeO_2 (Wu *et al.*, 2011) and $GeCl_4$ (Chou *et al.*, 2009) as precursors and result in similar particle sizes of around 5 nm.

For as-prepared Ge QDs, having an accurate atomic structure of nanoscale systems is a prerequisite to understanding their electronic and optical properties. Moreover, establishing a link between the structure and synthesis conditions is an essential requirement for the design of materials with predetermined properties. However, for ultra-small QDs, understanding the structure becomes complex due to the significant surface, interface (Weber *et al.*, 2013; Lee *et al.*, 2009; Pizzagalli *et al.*, 2001; Sato *et al.*, 1998) and size effects (Chiu *et al.*, 2006; Tomańek & Schluter, 1987). For example, Raman can be used to determine the size of nanocrystals employing the well known Richter model (Richter *et al.*, 1981; Campbell & Fauchet, 1986), but could be problematic for very small nanoparticles (Gouadec & Colomban, 2007). At the same time, XRD is not very informative for amorphous samples due to the broadening of diffraction peaks. Thus deducing an accurate structure (*i.e.* atomic arrangements and morphology) in small QDs is a non-trivial task that is still a challenge today.

In this paper we employed a combination of extended X-ray absorption fine structure (EXAFS), powder X-ray diffraction (PXRD), Raman and transmission electron microscope (TEM) techniques to examine the size and structure of matrix-free Ge QDs prepared by colloidal synthesis routes from GeO_2 and $GeCl_4$ in order to examine the influence of the precursor and synthesis conditions on the atomic structure and the surface of samples. We also looked into the effects of annealing on the structure of the produced Ge QDs.

2. Experiment

2.1. Synthesis

Two synthesis routes for Ge QDs were used. For the first route, bench-top colloidal synthesis (Wu *et al.*, 2011) was utilized to prepare Ge nanoparticles (NPs) by reduction of GeO_2 at 60°C at ambient pressure. In a typical experiment, GeO_2 powder (26 g, >99%) was dissolved in a solution of polyvinylpyrolidine (0.01 g, PVP, MW = 630.000) and of NaOH (10 ml, 0.15 *M*). Then HCl (0.5 ml, 0.5 *M*) was added to the flask to increase the pH to 7.0. At this point the solution is colourless and transparent. Heating the solution resulted in the formation of Ge nanoparticles by controlled addition of $NaBH_4$ (20 ml h^{-1} of 10 ml of 0.75 M) *via* a syringe pump. Over 30 min the colour of the solution changed from colourless to yellow, then brown and finally dark brown. All chemicals were purchased from Sigma-Aldrich and used as purchased without any purification. The formed Ge NPs were separated from the chemical residual using 10000 r.p.m. centrifugation and washed with ethanol several times. The formed Ge NPs were suspended in ethanol or kept in hexane. All samples were sealed in glass capillaries (0.7 mm) immediately after preparation to avoid prolonged exposure to air. The NPs produced *via* this synthesis route are referred to as Ca1.

For the second route, $GeCl_4$ (265 ml) was reduced with a solution of ethylene glycol (10 ml) and PVP (0.05 g, MW = 630.000) (Chou *et al.*, 2009). Then triglyme (6 ml) was added with two different rates: 90 ml h^{-1} for the first 2 ml and 9 ml h^{-1} for the remaining 4 ml. This controlled addition process of the triglyme was performed with a syringe pump into a three-neck round-bottom flask in which the solution is bubbled continuously with Ar gas or a mixture of H_2 and Ar gas from a micro-tube inlet through the solution. The final product was separated from the colloidal chemical solution by centrifugation at 10000 r.p.m. for 10 min. All samples were sealed in glass capillaries (0.7 mm) immediately after preparation to avoid prolonged exposure to air. The NPs produced *via* this synthesis route are referred to as Cs1.

In addition to the synthesis, the Ge QDs were annealed in H_2/Ar gas and Ar gas mediums at a flow rate of 100 ccm at temperatures of 450°C and 600°C for 1 h. All samples were annealed immediately following synthesis and were sealed in glass capillaries (0.7 mm) immediately after annealing.

2.2. Characterization

TEM (Jeol 2010) was employed to characterize the size distribution and morphology. Energy-dispersive X-ray spectroscopy (EDX) was used to analyse the component. Raman measurements were carried out using a Renishaw Raman microscope equipped with a 632 nm He–Ne laser. The experimental spectral resolution was 0.5 cm^{-1}. PXRD (performed at beamline B18, X-ray energy 8047 eV) and EXAFS measurement (performed at beamline B18, X-ray energy continuous from 10800 eV to 12400 eV with 0.88 eV resolution above the Ge *K*-absorption edge) was carried out at the Diamond synchrotron light source. For PXRD measurements a multi-channel curved detector was used. EXAFS measurements were carried out in transmission mode using ionization chambers. Reference data for bulk crystalline Ge were collected to obtain the value of the passive reduction factor S_0^2 that was later used in the analysis of EXAFS data from the samples. The passive reduction factor in diamond-type bulk Ge was found to be 0.94 ± 0.06.

The experimental EXAFS data were analysed using the software package *Demeter* (Newville *et al.*, 1995). The program *Athena* was used for background subtraction, where the same cut-off ('Rbkg' = 1.3) was used for all samples. EXAFS spectra were analyzed using the program *Artemis* with *FEFF* code for

scattering path calculation and the *FEFFIT* algorithm for fitting.

3. Results and discussion

TEM images for as-prepared Ca1 and Cs1 samples are shown in Figs. 1(*a*) and 1(*c*), respectively. The size distribution of as-prepared samples (both Ca1 and Cs1) was calculated from TEM images [Figs. 1(*b*) and 1(*d*), 60 particles were used to calculate the size distribution]. For Ca1 and Cs1 the QDs were found to have an average size of 3.8 ± 0.1 nm and 3.9 ± 0.1 nm, respectively. Raman spectra for as-prepared Ca1 and Cs1 samples are shown in Figs. 1(*e*) and 1(*f*). The observed peak can be assigned to the Ge–Ge vibration mode (around 300 cm^{-1} in bulk crystalline Ge). The asymmetry of the Raman peaks (49:27 and 44:16 at FWHM for Ca1 and Cs1, respectively), which is especially clear for the Cs1 sample (Fig. 1*f*), is due to particle size effects (Campbell & Fauchet, 1986; Richter *et al.*, 1981). The average particle sizes obtained from Raman using a fitting based on the phonon confinement model (Campbell & Fauchet, 1986; Richter *et al.*, 1981) for Ca1 and Cs1 are 2.6 ± 0.5 nm and 3.2 ± 0.5 nm, respectively. This is in contrast to the TEM data where observed sample sizes are very similar. For Cs1, the particle sizes obtained from TEM and Raman are similar. However, there is a clear discrepancy between Raman and TEM size analysis in Ca1. In both samples the Raman peaks are downshifted (as compared with the bulk c-Ge) as expected, but the broader peak observed in the spectrum of Ca1 may suggest a higher amorphous component. This would explain the discrepancy in sizes calculated from TEM (Fig. 1*b*) and Raman (Fig. 1*e*) since the quantum confinement model for particle size calculation (Campbell & Fauchet, 1986; Richter *et al.*, 1981) assumes a crystalline sample. Furthermore, contribution from the amorphous content (higher in Ca1) to the Raman signal may explain much less pronounced asymmetry of the signal from Ca1 sample as compared with Cs1.

PXRD measurements were carried out to obtain long-range order information. Fig. 2 presents background-subtracted diffraction patterns for all Ca1 and Cs1 samples. Ca1 (GeO_2 precursor) and Cs1 ($GeCl_4$ precursor) as-prepared samples both show broad diffraction features typical of small nanoparticles (or amorphous samples). However, the average peak positions are clearly different as can be seen in Figs. 2(*a*), 2(*b*), 2(*d*) and 2(*e*), where numerical values for the peak positions and of the FWHM are also shown, assuming Gaussian peak profile. Analysis of the FWHM of XRD peaks in the 20–30° range suggests a higher degree of disorder in as-prepared Ca1 (FWHM of 8.7–9.6°) samples compared with as-prepared Cs1 (FWHM of 5.4–6.1°). This is consistent with the Raman data shown earlier. However, FWHM for both samples are smaller than that of around 15° normally observed in bulk (Muthuswamy *et al.*, 2013) or thin-film (Khan *et al.*, 2010*a*,*b*) amorphous Ge. Thus, XRD data suggest a higher degree of long-range order in all our as-prepared Ge QDs than in an amorphous Ge phase.

Detailed comparison of *d*-spacing between experimental data and the reference (Ge and GeO_2 related) can be found

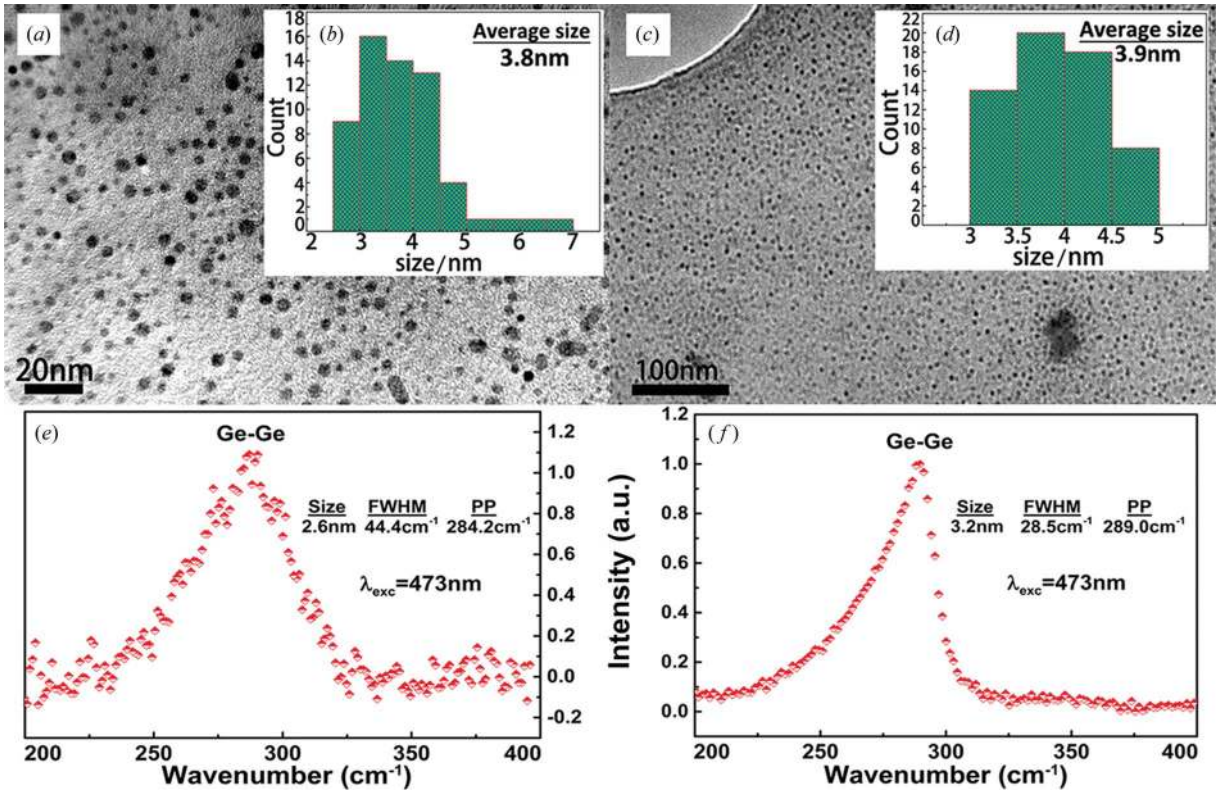

Figure 1
(*a*, *b*) TEM and size distribution of Ca1 as-prepared sample; (*c*, *d*) TEM and size distribution of Cs1 as-prepared sample; (*e*, *f*) Raman spectrum for Ca1 and Cs1 as-prepared samples, respectively.

Table 1
d-spacings (in Å) calculated from PXRD patterns compared with the JCPDS database for α-quartz, rutile GeO_2 and diamond-type Ge.

Sample	Experiment	α-Quartz GeO_2 (JCPDS No. 361463)	Rutile GeO_2 (JCPDS No. 710651.)	Diamond Ge (JCPDS No. 4-545)
Ca1 Hex Ar	3.21 ± 0.03	3.43, (101)	3.11, (110)	3.25, (111)
	2.13 ± 0.01	2.16, (202)	2.11, (111)	2.00, (220)
Ca1 Hex H_2Ar	3.28 ± 0.03	3.43, (101)	3.11, (110)	3.25, (111)
Ca1 annealed 450	4.65 ± 0.06	4.32, (110)	NA	NA
	3.27 ± 0.03	3.43, (101)	3.11, (110)	3.25, (111)
	2.00 ± 0.01	2.02, (201)	1.97, (210)	2.00, (220)
	1.70 ± 0.01	1.73, (202)	NA	1.70, (311)
Ca1 annealed 600	3.27 ± 0.03	3.43, (101)	3.11, (110)	3.25, (111)
	2.82 ± 0.02	2.49, (2$\bar{1}$0)	NA	NA
	2.00 ± 0.01	2.02, (201)	1.97, (210)	2.00, (220)
	1.70 ± 0.01	1.73, (20$\bar{2}$)	NA	1.70, (311)
	1.63 ± 0.01	1.63, (3$\bar{1}$0)	1.62, (212)	NA
Cs1 Hex Ar	3.97 ± 0.04	4.32, (110)	NA	NA
Cs1 Hex H_2Ar	3.97 ± 0.04	4.32, (110)	NA	NA
Cs1 annealed 450	4.67 ± 0.06	4.32, (110)	NA	NA
	3.27 ± 0.03	3.43, (101)	3.11, (110)	3.25, (111)
	2.82 ± 0.02	2.49, (2$\bar{1}$0)	NA	NA
	2.00 ± 0.01	2.02, (201)	1.97, (210)	2.00, (220)
	1.70 ± 0.01	1.73, (20$\bar{2}$)	NA	1.70, (311)
	1.63 ± 0.01	1.63, (3$\bar{1}$0)	1.62, (212)	NA

in Table 1. The position of the first broad peak in PXRD data for Ca1 (corresponding to a distance of around 3.28 Å) is consistent with the distance corresponding to the (111) plane of diamond-type (JCPDS No. 4-545) Ge structure. However, the peak position is different for Cs1 as-prepared samples, as it corresponds to a distance of around 3.97 Å (see Table 1). This result is contrary to the XRD data previously reported for this synthesis route (Chou *et al.*, 2009), but similar to the recently reported XRD data recorded for nanocrystalline Ge prepared by laser ablation (Liu *et al.*, 2013).

We compared the PXRD signal for Cs1 samples with a number of relevant metastable Ge phases [ST12 (Kasper & Richards, 1964), mC16 (Selli *et al.*, 2013) and BC8 (Nelmes *et al.*, 1993)] in order to understand possible origins of the peak position. Our data together with the corresponding PXRD simulated for several Ge phases are shown in Fig. 3. One can see that out of all phases only the recently reported mC16 phase (Selli *et al.*, 2013) has several diffraction peaks that fall within the range of the observed broad peak.

We further investigated the effects of annealing on the structure of as-prepared Ge QDs. As seen in Fig. 2, annealing results in crystallization of as-prepared Ca1 and Cs1 samples into diamond-type Ge. However, in all cases there are extra diffraction features present. These diffraction peaks, labelled with arrows, for Ca1 annealed 600 and Cs1 annealed 450 (samples annealed at 450°C and 600°C, see §2) are not from diamond-type Ge. EDX measurements were carried out for these two samples to check impurities beyond Ge. Results show that these two annealed samples are both mainly composed of Ge, C (from the TEM grid) and O, which suggests that the two extra diffraction peaks can only come from a Ge-related phase.

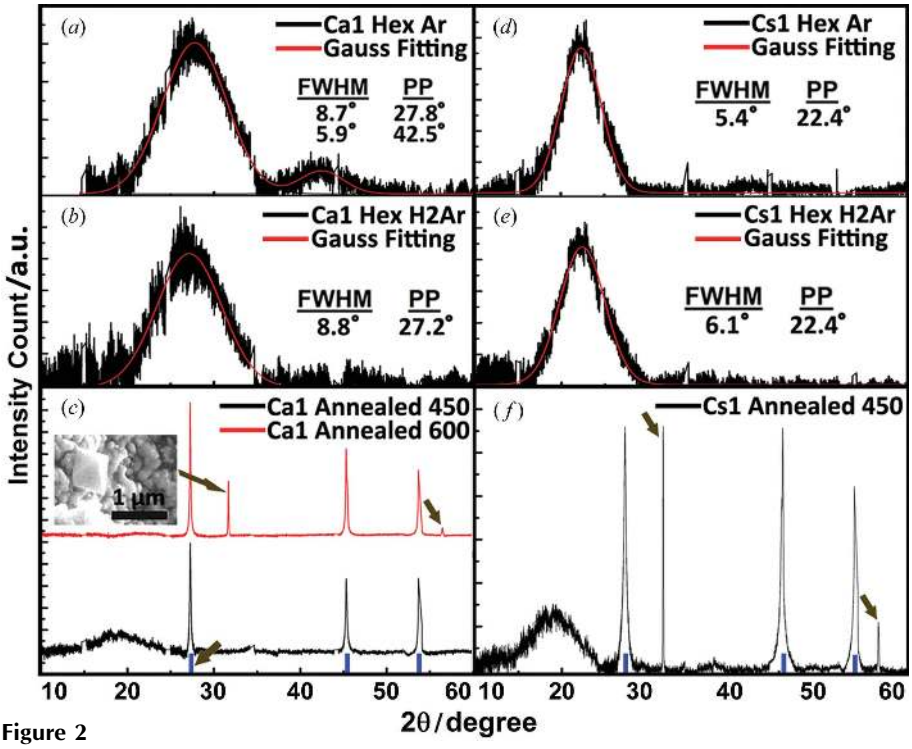

Figure 2
Background-subtracted PXRD patterns for all as-prepared and annealed Ca1 (*a*–*c*) and Cs1 (*d*–*f*) samples; reference for diamond-type Ge (JCPDS No. 4-545) is shown as blue marks at the bottom. 'Hex' in the sample name means a suspension in hexane, and 'Eth' for ethanol; 'Ar' means synthesis with Ar gas protection and 'H_2Ar' for a mixture of H_2 and Ar. The background was subtracted using PXRD measurement of an empty capillary. The inset image is SEM for Ca1 annealed 600.

Further comparison (see Table 2) with relevant Ge metastable phases suggests that these reflections are close to those found in the BC8 (cubic unit cell) phase. Interestingly, the inset (Fig. 2) scanning electron microscope (SEM) image for Ca1 annealed 600 shows a pyramid of large size (around 1 μm), which could explain the sharpness of the arrow-labelled diffraction peak, while the pyramid shape is not inconsistent with a BC8 structure.

EXAFS measurements at the Ge *K*-edge were performed to determine the local atomic arrangements and to gain information on the local atomic distortions and possible surface termination since the technique selectively probes the environment of Ge atoms. EXAFS spectra were transformed into pseudo radial distribution functions to visualize the structural data (Fig. 4: Ca1; Fig. 5:

Table 2
Comparison of two extra diffraction peaks in Ca1 annealed samples with Ge metastable phases.

Experiment	BC8, Ge	ST12, Ge	mC16, Ge
2.82 Å	2.83 Å, (112)	2.73 Å, (201)	2.77 Å, (0-22)
1.63 Å	1.63 Å, (114)	1.64 Å, (320)	1.62 Å, (4-22)

Cs1). For as-prepared Ca1 (GeO_2 precursor) samples, a clear signal from Ge—O bonding was observed. We conclude that Ge—O bonding is most likely to be associated with the surface, since no signal corresponding to Ge—O—Ge bonding (3.066 or 3.221 Å) (Baur & Khan, 1971) was observed in EXAFS and no reflections were found corresponding to GeO_2 in PXRD. Moreover, one can clearly see [Figs. 4(*a*) and 4(*b*)] that this feature is stronger for the sample where Ar rather than H_2Ar gas was used. By using the *FEFFIT* algorithm, the fitted Ge—O bonding length (around 1.78 Å, Table 3) is found to be close to the bond length (1.87 Å) in rutile-type (Bolzan *et al.*, 1997) GeO_2. A Debye correlated model was used to fit the Ge—Ge shell. From Table 3 it can be inferred that the fitted Debye temperature is close to the theoretical value of bulk Ge (373 K) (Stewart, 1983). The fitted Ge—Ge bond length is around 2.45 Å, which is consistent with that of diamond-type Ge. EXAFS results suggest that a GeO_2 shell may contribute to the overall particle size and thus further explain the size discrepancy between the TEM result and Raman calculation for as-prepared Ca1 sample.

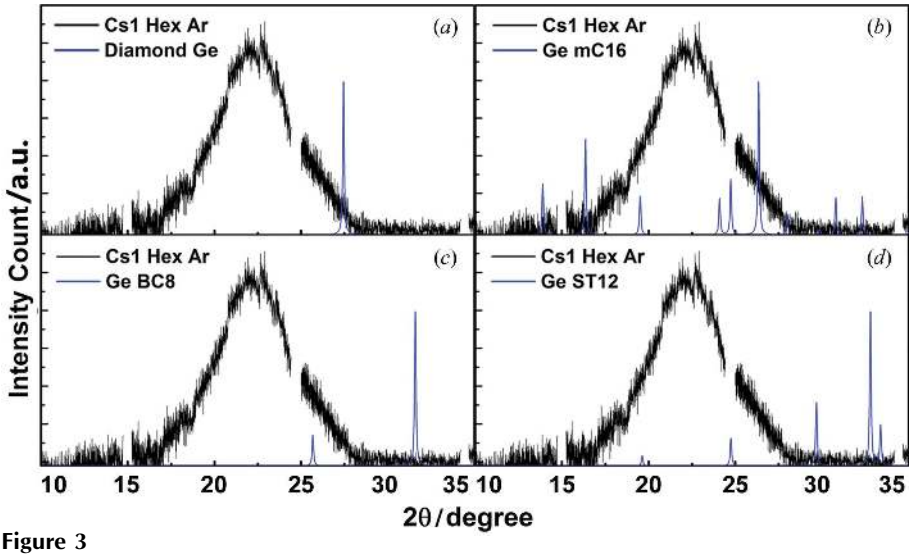

Figure 3
Comparison of Cs1 as-prepared sample PXRD pattern with Ge related phase: (*a*) diamond; (*b*) mC16; (*c*) BC8; (*d*) ST12. Gaps in the original data are due to dead areas between XRD detector segments.

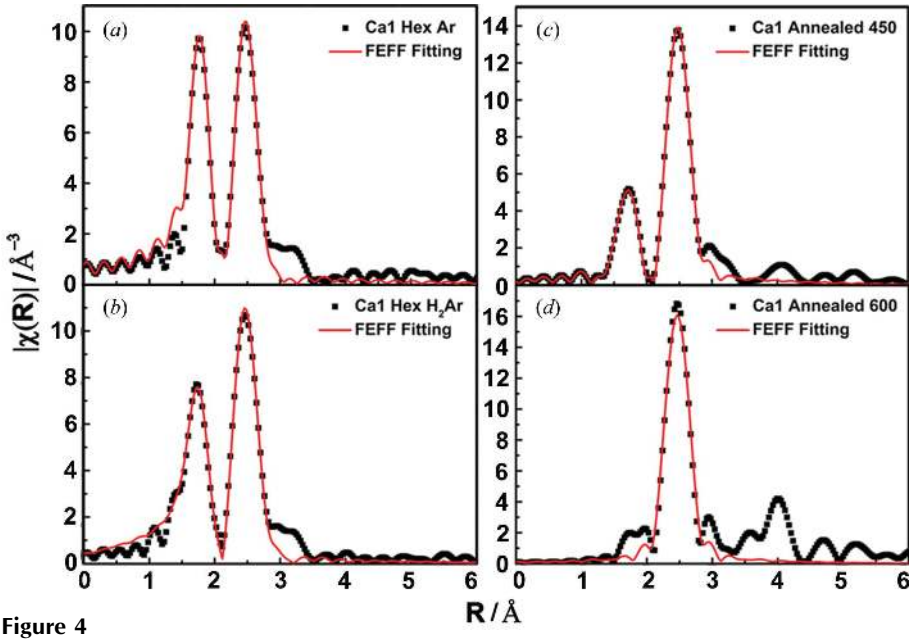

Figure 4
(*a*, *b*) EXAFS fitting result for Ca1 Hex Ar and Ca1 Hex H_2Ar, respectively; (*c*, *d*) EXAFS fitting result for Ca1 Ar annealed 450 and Ca1 Ar annealed 600, respectively.

For as-prepared Cs1 (see Fig. 5), no other bonding features beyond Ge—Ge were observed. Considering the details of synthesis routes and that the surface of the samples must be terminated, we suggest that the surface of as-prepared Cs1 is most likely to be terminated with hydrogen, which cannot be seen by EXAFS measurements due to the weak scattering by hydrogen atoms. As seen in Table 4, the fitted Ge—Ge interatomic distance of 2.42 ± 0.02 Å (or 2.43 ± 0.02 Å) is somewhat shorter than 2.45 Å for diamond and 2.48 Å for both ST12 and BC8. However, an interatomic distance of 2.42 Å is found in the mC16 phase, which could possibly account for the detected Ge—Ge bonding length and would be consistent with the PXRD analysis of as-prepared Cs1.

For most annealed samples the fitted Ge—Ge interatomic distances correspond well with that of diamond Ge. For Ca1 annealed 450, the slightly larger Ge—Ge bonding should be due to the average of the contributions from the crystalline and amorphous parts, since as-prepared Ca1 shows larger first-shell bonding (2.48 Å). However, for the first Ge—Ge shell of Ca1 annealed 600 and Cs1 annealed 450, the fitted Debye–Waller factor does not decrease by any significant degree upon annealing (see Table 3) as would be expected. Debye–Waller factors include dynamic and static contributions. The dynamic contribution is not expected to change as it is primarily defined by the nature of the bond. Hence a significant amount of static distortion should still exist in annealed samples. This static disorder

Table 3
EXAFS fitting result for Ca1 samples.

For Ge—Ge bonding, the Debye correlated model was used for fitting, so the error was only provided for the Debye temperature but not for the Debye–Waller factor (σ^2). For the Ca1 annealed 600 sample, the Debye temperature was fixed at 370 K to avoid non-physical fitting result. R_{eff} for diamond Ge: first shell 2.45 Å; for rutile GeO_2: first shell 1.87 Å.

Sample	Debye temperature (K)	σ^2 Ge—Ge (Å^2)	R (Ge—Ge) (Å)	Coordination number	R (Ge—O) (Å)
Ca1 Hex Ar	325.3 ± 25.1	0.006	2.46 ± 0.01	2.5 ± 0.5	1.78 ± 0.01
Ca1 Hex H_2Ar	309.8 ± 18.3	0.007	2.45 ± 0.01	2.9 ± 0.4	1.77 ± 0.01
Ca1 annealed 450	355.6 ± 22.6	0.005	2.46 ± 0.01	2.9 ± 0.4	1.76 ± 0.01
Ca1 annealed 600	370	0.005	2.45 ± 0.01	3.2 ± 0.4	NA

Table 4
EXAFS fitting result for Cs1 samples.

Sample	Debye temperature Ge (K)	σ^2 Ge—Ge (Å^2)	R_{eff} (Ge—Ge) (Å)	R (Ge—Ge (Å)	Coordination number
Cs1 Hex Ar	349.4 ± 16.8	0.005	2.4, Dia 2.48, BC8	2.42 ± 0.02	3.3 ± 0.4
Cs1 Hex H_2Ar	344.7 ± 22.7	0.006	2.48, ST12 2.42, mC16	2.43 ± 0.02	3.8 ± 0.5
Cs1 annealed 450	381.6 ± 27.4	0.005	2.45, Dia	2.45 ± 0.02	3.2 ± 0.4

can originate from distortions within tetrahedrons composed of local Ge atoms [red arrow in Fig. 5(*d*)], but can also be an indication of phases other than diamond-type Ge being present. The latter is consistent with the analysis of PXRD data.

The first-shell coordination numbers are shown in Tables 3 and 4 for all as-prepared and annealed samples. The extracted coordination numbers were found to be lower than that of various Ge theoretical phases (diamond: 4 at 2.45 Å; BC8: 1 at 2.41 Å, 3 at 2.50 Å; mC16: 3 at 2.42 Å, 1 at 2.45 Å; ST12: 4 at 2.48 Å). This is most likely due to the combination of large surface-to-volume ratios in nanoparticles and a correlation between Debye temperature and coordination numbers during data fitting. Neither of these factors affect the extracted interatomic distances.

Based on the comprehensive analysis above, it is suggested that two different synthesis routes seem to produce samples with a large degree of structural disorder and distinctly different metastable phases. On annealing, samples transform into crystalline diamond-type Ge, again with the possible presence of metastable phases.

There could be several possibilities for the morphology of as-prepared Ca1 and Cs1 Ge nanoparticles (see Fig. 6). First of all, the discrepancy of sizes extracted from TEM and Raman indicates that a disordered component is present in our sample, which is consistent with PXRD data. Then PXRD patterns suggest that the long-range order in our as-prepared Ge QDs is better than that in amorphous Ge. Thus TEM/Raman/PXRD results comprehensively exclude cases (*a*) and (*b*) in Fig. 6. Moreover, the size discrepancy between TEM and Raman for Ca1 could also come from GeO_2 on the surface. Furthermore, a mixture of independent nano-crystalline and nano-amorphous QDs with the particle size observed in TEM [case (*c*), Fig. 6] would result in the observation of second (and possibly further) coordination shells in EXAFS data, which is not the case for as-prepared samples. Besides, a mixture of crystalline and amorphous Ge QDs would result in a non-Gaussian peak shape (broad amorphous background with a sharp crystalline peak on top) rather than the Gaussian diffraction peak we observed. A mixed phase [case (*d*), Fig. 6] in a single QD with size down to sub-nanometres can be excluded on the basis of thermodynamic considerations (De Yoreo & Vekilov, 2003; Weeks & Gilmer, 2007).

Hence the most likely model for as-prepared Ge QDs is a core-shell one shown in Fig. 6(*e*). This has been predicted from first-principle and molecular dynamics calculations (Pizzagalli *et al.*, 2001; Pizzagalli & Galli, 2002), but has not been confirmed

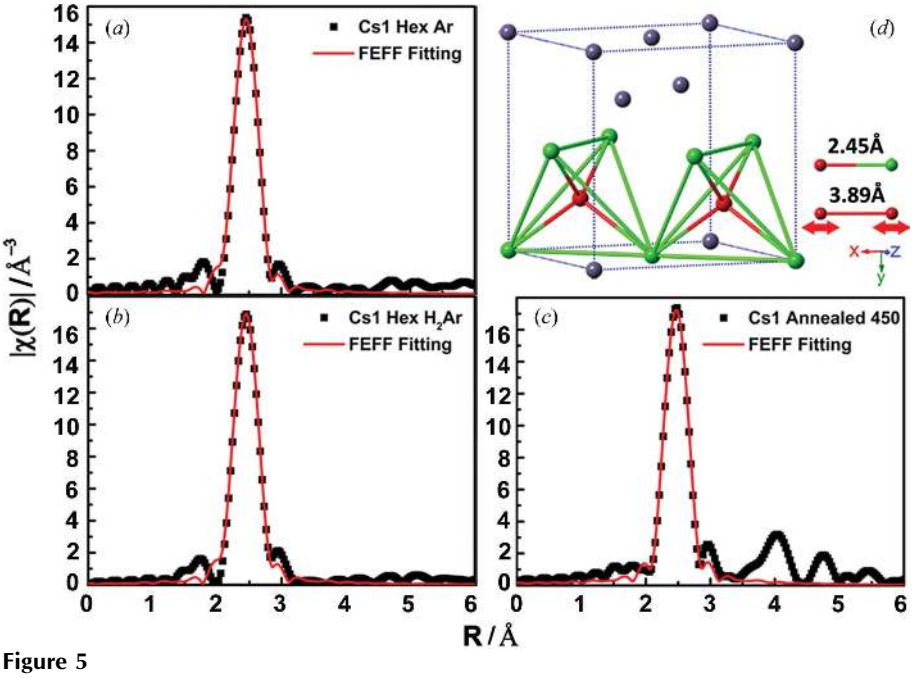

Figure 5
(*a*, *b*) EXAFS fitting result for Cs1 Hex Ar, Cs1 Hex Ar, respectively; (*c*) EXAFS fitting result for Cs1 annealed 450. (*d*) The unit cell of diamond and ST12 Ge (including polyhedron based on local tetragonal structure) is shown.

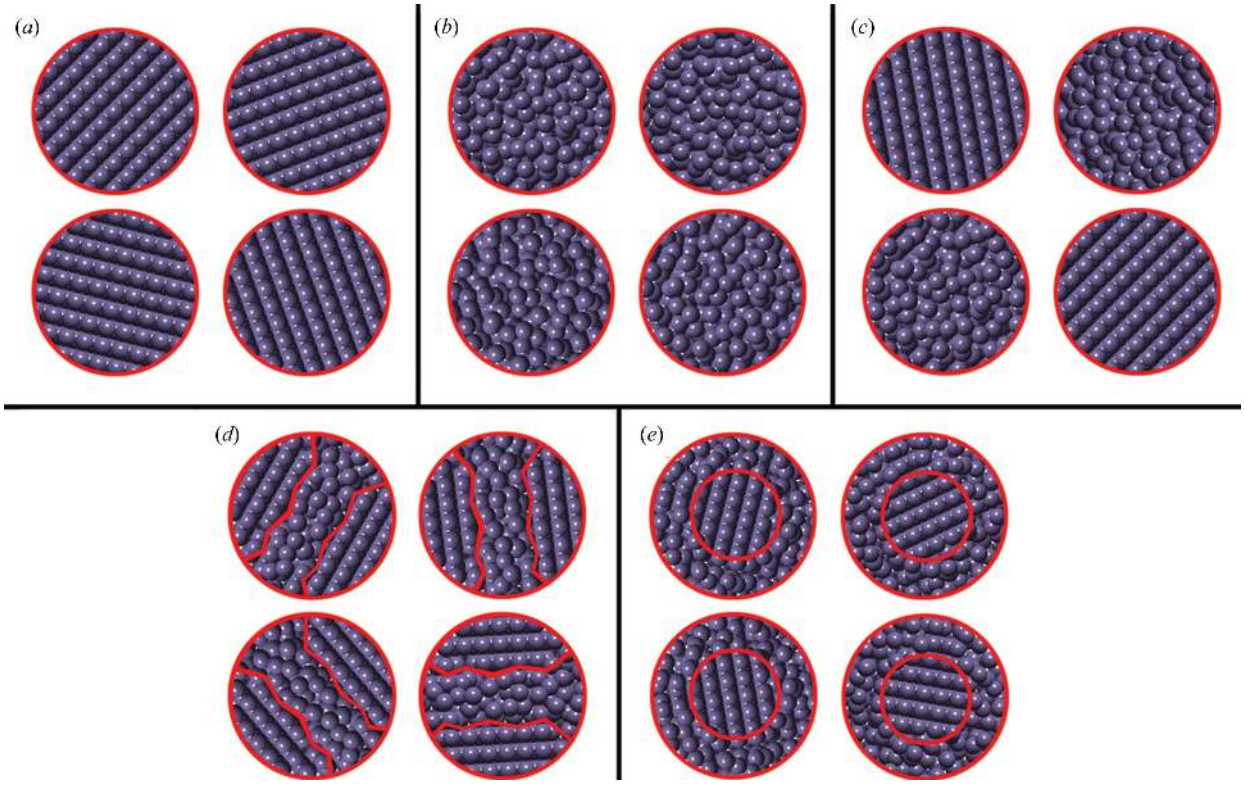

Figure 6
Five general possibilities for as-prepared homogeneous and inhomogeneous Ge QDs. (*a*) Crystalline. (*b*) Amorphous. (*c*) Mixture of crystalline and amorphous QDs. (*d*) Mixed crystalline–amorphous within one single QD. (*e*) Single QD with nano-crystalline core and amorphous shell.

by experimental data until now for colloidal Ge QDs. For Ca1 as-prepared QDs, the surface could possibly be terminated with a GeO_2 shell based on EXAFS/TEM/Raman analysis. We believe Cs1 as-prepared samples are terminated with hydrogen.

4. Conclusion

Ge QDs were synthesized by two colloidal routes: one of which by reducing GeO_2 (Ca1 route) and the other by reducing $GeCl_4$ (Cs1 route). Combined EXAFS/PXRD/Raman/TEM characterization was carried out to reveal the short- and long-range order, and to access information on the atomic structure of the samples. It was found that as-prepared Ca1 has diamond-type Ge structure with oxide-terminated surface. More interestingly, PXRD and EXAFS data for as-prepared Cs1 suggest a metastable phase different from that found in Ca1. This metastable phase seems to correspond best to the recently suggested (on the basis of calculations) Ge mC16 structure, with the surface most likely terminated by hydrogen. These results suggest that metastable phases of Ge can be obtained by a suitable choice of precursors and be influenced by the size and possibly by surface termination, thus giving access to novel structures otherwise available only under extreme conditions of pressure and temperature (Hanfland & Syassen, 1990; Nelmes *et al.*, 1993). Further comprehensive EXAFS/PXRD analysis for Ca1 and Cs1 as-prepared and annealed samples reveals phase transitions and the coexistence of diamond and metastable Ge phases upon annealing. The comprehensive results from Raman, TEM, PXRD and EXAFS suggest the core-shell model for the morphology of both as-prepared Ca1 and Cs1.

This research was supported by Queen Mary, University of London. We would like to thank Diamond synchrotron light source for the beamline (B18) and the corporation work. AK and OE acknowledge the Turkish Ministry of National Education. WL is grateful to the South East Physics Network (SEPnet). YZ was supported by Chinese Scholarship Council (CSC) for PhD study.

References

Alkis, S., Ghaffari, M. & Okyay, A. K. (2012). *Mater. Chem. Phys.* **134**, 616–622.
Assefa, S., Xia, F. N. A. & Vlasov, Y. A. (2010). *Nature (London)*, **464**, 80–84.
Baur, W. H. & Khan, A. A. (1971). *Acta Cryst.* B**27**, 2133–2139.
Bolzan, A. A., Fong, C., Kennedy, B. J. & Howard, C. J. (1997). *Acta Cryst.* B**53**, 373–380.
Brus, L. E. (1983). *J. Chem. Phys.* **79**, 5566–5571.
Campbell, I. H. & Fauchet, P. M. (1986). *Solid State Commun.* **58**, 739–741.
Cánovas, E., Fuertes Marrón, D. F., Martí, A., Luque, A., Bett, A. W., Dimroth, F. & Philipps, S. P. (2010). *Appl. Phys. Lett.* **97**, 203504.
Chiu, H. W., Chervin, C. N. & Kauzlarich, S. M. (2005). *Chem. Mater.* **17**, 4858–4864.
Chiu, H. W., Kauzlarich, S. M. & Sutter, E. (2006). *Langmuir*, **22**, 5455–5458.
Chou, N. H., Oyler, K. D., Motl, N. E. & Schaak, R. E. (2009). *Chem. Mater.* **21**, 4105–4107.

Cojocaru, C. V., Bernardi, A., Reparaz, J. S., Alonso, M. I., MacLeod, J. M., Harnagea, C. & Rosei, F. (2007). *Appl. Phys. Lett.* **91**, 113112.

Dag, O., Henderson, E. J. & Ozin, G. A. (2012). *Small*, **8**, 921–929.

Desnica, U. V., Salamon, K., Buljan, M., Dubcek, P., Radic, N., Desnica-Frankovic, I. D., Siketic, Z., Bogdanovic Radovic, I., Ivanda, M. & Bernstorff, S. (2008). *Superlattice Microstruct.* **44**, 323–330.

De Yoreo, J. J. & Vekilov, P. G. (2003). *Rev. Mineral. Geochem.* **54**, 57–93.

Einevoll, G. T. (1992). *Phys. Rev. B*, **45**, 3410–3417.

Fan, J. Y. & Chu, P. K. (2010). *Small*, **6**, 2080–2098.

Fok, E., Shih, M. L., Meldrum, A. & Veinot, J. G. C. (2004). *Chem. Commun.* pp. 386–387.

Gerung, H., Bunge, S. D., Boyle, T. J., Brinker, C. J. & Han, S. M. (2005). *Chem. Commun.* **14**, 1914–1916.

Gouadec, G. & Colomban, P. (2007). *Prog. Cryst. Growth Charact. Mater.* **53**, 1–56.

Guter, W., Schöne, J., Philipps, S. P., Steiner, M., Siefer, G., Wekkeli, A., Welser, E., Oliva, E., Bett, A. W. & Dimroth, F. (2009). *Appl. Phys. Lett.* **94**, 223504.

Hanfland, M. & Syassen, K. (1990). *High. Press. Res.* **3**, 242–244.

Heath, J. R., Shiang, J. J. & Alivisatos, A. P. (1994). *J. Chem. Phys.* **101**, 1607–1615.

Henderson, E. J., Seino, M., Puzzo, D. P. & Ozin, G. A. (2010). *ACS Nano*, **4**, 7683–7691.

Hope-Weeks, L. J. (2003). *Chem. Commun.* pp. 2980–2981.

Jamieson, J. C. (1963). *Science*, **139**, 762–764.

Joannopoulos, J. & Cohen, M. L. (1973). *Phys. Rev. B*, **8**, 2733–2755.

Kamata, Y. (2008). *Mater. Today*, **11**, 30–38.

Kartopu, G., Bayliss, S. C., Karavanskii, V. A., Curry, R. J., Turan, R. & Sapelkin, A. V. (2003). *J. Lumin.* **101**, 275–283.

Kartopu, G., Sapelkin, A. V., Karavanskii, V. A., Serincan, U. & Turan, R. (2008). *J. Appl. Phys.* **103**, 113518.

Kasper, J. S. & Richards, S. M. (1964). *Science*, **17**, 752–755.

Khan, A. F., Mehmood, M., Aslam, M. & Shah, S. I. (2010). *J. Colloid Interface Sci.* **343**, 271–280.

Khan, A. F., Mehmood, M., Rana, A. M. & Muhammad, T. (2010). *Appl. Surf. Sci.* **256**, 2031–2037.

Kim, S. J., Quy, O. K., Chang, L. S., Stach, E. A., Handwerker, C. A. & Wei, A. (2010). *J. Mater. Chem.* **20**, 331–337.

Lambert, T. N., Andrews, N. L., Gerung, H., Boyle, T. J., Oliver, J. M., Wilson, B. S. & Han, S. M. (2007). *Small*, **3**, 691–699.

Lambert, T. N., Gerung, H., Boyle, T. J., Andrews, N. L., Tribby, L. J., Oliver, J. M., Brinker, C. J. & Han, S. M. (2006). *231st National Meeting of the American Chemical Society, Abstracts of the Papers of the American Chemical Society.* Atlanta, GA, USA.

Lee, D. C., Pietryga, J. M., Robel, I., Werder, D. J., Schaller, R. D. & Klimov, V. I. (2009). *J. Am. Chem. Soc.* **131**, 3436–3437.

Liu, J., Liang, C. H., Tian, Z. F., Zhang, S. Y. & Shao, G. S. (2013). *Sci. Rep.* **3**, 1741.

MacLeod, J. M., Cojocaru, C. V., Ratto, F., Harnagea, C., Bernardi, A., Alonso, M. I. & Rosei, F. (2012). *Nanotechnology*, **23**, 065603.

Muthuswamy, E., Iskandar, A. S., Amador, M. M. & Kauzlarich, S. M. (2013). *Chem. Mater.* **25**, 1416–1422.

Muthuswamy, E., Kauzlarich, S. M. & Susan, M. (2012). *Symposium on Ionic Liquids-Science and Applications, 243rd National Spring Meeting of the American Chemical Society.* San Diego, CA, USA.

Nelmes, R. J., McMahon, M. I., Wright, N. G., Allan, D. R. & Loveday, J. S. (1993). *Phys. Rev. B*, **48**, 9883–9886.

Newville, M., Ravel, B., Haskel, D., Rehr, J. J., Stern, E. A. & Yacoby, Y. (1995). *Physica B*, **208**, 154–156.

Nogami, M. & Abe, Y. (1997). *J. Sol-Gel Sci. Technol.* **8**, 867–870.

Park, K., Lee, Y., Lee, J. & Lim, S. (2008). *Appl. Surf. Sci.* **254**, 4828–4832.

Peng, C. Z., Gao, J., Wang, S. D., Zhang, X. H., Zhang, X. P. & Sun, X. H. (2011). *J. Phys. Chem. C*, **115**, 3866–3871.

Pillarisetty, R. (2011). *Nature (London)*, **479**, 324–328.

Pizzagalli, L. & Galli, G. (2002). *Mater. Sci. Eng. B*, **96**, 86–89.

Pizzagalli, L., Galli, G., Klepeis, J. E. & Gygi, F. (2001). *Phys. Rev. B*, **63**, 165324.

Prabakar, S., Shiohara, A., Hanada, S., Fujioka, K., Yamamoto, K. & Tilley, R. D. (2010). *Chem. Mater.* **22**, 482–486.

Ribeiro, F. J. & Cohen, M. L. (2000). *Phys. Rev. B*, **62**, 11388–11391.

Richter, H., Wang, Z. P. & Ley, L. (1981). *Solid State Commun.* **39**, 625–629.

Rivillon, S., Chabal, Y. J., Amy, F. & Kahn, A. (2005). *Appl. Phys. Lett.* **87**, 253101.

Sato, S., Nozaki, S. & Morisaki, H. (1998). *Appl. Phys. Lett.* **72**, 2460–2462.

Selli, D., Baburin, I. A., Martonak, R. & Leoni, S. (2013). *Sci. Rep.* **3**, 1466.

Stavarache, I., Lepadatu, A. M., Gheorghe, N. G., Costescu, R. M., Stan, G. E., Marcov, D., Slav, A., Iordache, G., Stoica, T. F., Iancu, V., Teodorescu, V. S., Teodorescu, C. M. & Ciurea, M. L. (2011). *J. Nanopart. Res.* **13**, 221–232.

Stewart, G. R. (1983). *Rev. Sci. Instrum.* **54**, 1–11.

Tomańek, D. & Schluter, M. A. (1987). *Phys. Rev. B*, **36**, 1208–1217.

Weber, J. R., Janotti, A. & Van de Walle, C. G. (2013). *Phys. Rev. B*, **87**, 035203.

Weeks, J. D. & Gilmer, G. H. (2007). *Adv. Chem. Phys.* pp. 157–228. New York: John Wiley and Sons.

Welham, N. J. (2000). *J. Mater. Res.* **15**, 2400–2407.

Wu, H. P., Liu, J. F., Wang, Y. W., Zeng, Y. W. & Jiang, J. Z. (2006). *Mater. Lett.* **60**, 986–989.

Wu, J. H., Sun, Y. G., Zou, R. J., Song, G. S., Chen, Z. G., Wang, C. R. & Hu, J. Q. (2011). *CrystEngComm*, **13**, 3674–3677.

Xue, D. J., Wang, J. J., Wang, Y. Q., Xin, S., Guo, Y. G. & Wan, L. J. (2011). *Adv. Mater.* **23**, 3704–3707.

Yang, L. (2007). Thesis, University of Bristol, UK.

Yin, M. T. & Cohen, M. L. (1980). *Phys. Rev. Lett.* **45**, 1004–1007.

Zaitseva, N., Dai, Z. R., Grant, C. D., Harper, J. & Saw, C. (2007). *Chem. Mater.* **19**, 5174–5178.